ISSN (Print) 1226-1750
ISSN (Online) 2233-6656
Journal of Magnetics 24(2), 223-229 (2019) https://doi.org/10.4283/JMAG.2019.24.2.223

Development and Application of a Deep Convolutional Neural Network Noise Reduction Algorithm for Diffusion-weighted Magnetic Resonance Imaging

Dong-Kyoon Han[1], Kyuseok Kim[2], and Youngjin Lee[3]*

[1]*Department of Radiological Science, Eulji University, Gyeonggi-do 13135, Republic of Korea*
[2]*Department of Radiation Convergence Engineering, Yonsei University, Gangwon-do 26493, Republic of Korea*
[3]*Department of Radiological Science, Gachon University, Incheon 21936, Republic of Korea*

(Received 27 March 2019, Received in final form 24 April 2019, Accepted 24 April 2019)

Diffusion-weighted imaging (DWI) is frequently used in the field of diagnostic medicine to detect various human diseases. In DWI, noise suppression is very important for achieving high detection accuracy of diseases. In this study, we develop a deep convolutional neural network (Deep-CNN) noise reduction algorithm and evaluate its effectiveness in DWI by performing both simulations and real experiments with a 1.5- and a 3.0-T MRI system. The results validate the proposed Deep-CNN algorithm for DWI. Compared with previously developed non-local means (NLM) algorithms, the proposed Deep-CNN algorithm achieves superior quantitative results. In conclusion, the quantitative results verify that the proposed Deep-CNN algorithm has higher noise reduction efficiency and image visibility than previously developed algorithms for DWI.

Keywords : Deep convolutional neural network (Deep-CNN) noise reduction algorithm, Diffusion-weighted imaging (DWI), Magnetic resonance imaging (MRI), Image processing, quantitative evaluation of image performance

1. Introduction

Medical imaging has become an integral technique for early detection of diseases [1, 2]. Although X-ray based imaging systems, such as X-ray radiography and computed tomography (CT), are important tools in medicine, they present the issue of patients' exposure to dangerous ionizing radiation, that is high energy wavelengths [3]. Among medical imaging techniques, magnetic resonance imaging (MRI), which can produce images in any plane with no exposure to ionizing radiation, is being used increasingly [4-6]. In particular, the advantage of MRI compared to X-ray based imaging systems is the excellent image quality, in terms of contrast and spatial resolution [7].

In MRI techniques, diffusion-weighted imaging (DWI), which is based on the molecular diffusion effect, *i.e.*, the random movement of molecules (water) in tissues, can achieve early detection of diseases or subtle changes in the body. It is being increasingly applied in a variety of medical diagnosis fields, including brain and musculoskeletal applications, owing to its improved gradient performance and the development of MRI multichannel surface coils [8, 9]. To perform DWI, a very strong pair of gradient magnetic fields (diffusion-weighted gradient fields) is needed in addition to the main magnetic field, which is essential for acquiring an image. The integral of the intensity and time of the diffusion-weighted gradient fields is called the gradient factor or the b-value, and the numerical value of the degree of diffusion of water is referred to as the apparent diffusion coefficient (ADC), which is based on a quantitative measure of tissue diffusivity [8]. Both ADC map-based and diffusion-weighted images are valuable in the localization of diseases [10]. In particular, the b-value identifies the sensitivity calculation to diffusion and is calculated as follows:

$$b-\text{value}(s/mm^2) = G^2A^2\zeta^2(\Delta-\zeta/3), \quad (1)$$

where G is the gyromagnetic ratio, A is the amplitude of the two diffusion gradient pulses, ς is the pulse duration, and Δ is the time between the two pulses.

The model of the signal intensity with respect to the b-value can be fitted to each result image. According to a research by M. C. Mass et al., the image noise depends strongly on the b-value in both simulations and real experiments with 1.5- and 3.0-T MRI systems [11]. Thus, the b-value is very important in DWI to reduce image

*Corresponding author: Tel: +82-32-820-4362
Fax: +82-32-820-4531, e-mail: yj20@gachon.ac.kr

noise and hence analyze images.

Many image processing approaches have been developed to reduce noise. To effort for the noise suppression for noise, a variety of algorithm introduced such as total variation filtering, wavelet filtering, *etc* [12, 13]. Buades *et al.* introduce the non-local means (NLM) algorithm [14] recently and shown the outstanding results. Its algorithm implemented the noise suppression through calculating the mean values at selected the local patches based on an assumption of self-similarity exist in the noisy image. However, these methods based on the filtering have inherent problem; decreasing the spatial resolution by smoothing while the filter calculate. Recently, noise reduction algorithms based on deep convolutional neural networks (Deep-CNN) with machine-learning have been developed. In a previous study, a research group proposed a noise reduction method for low dose CT systems and demonstrated that the peak signal to noise ratio using a Deep-CNN algorithm was approximately 1.02 times higher than that of a high-efficiency total variation algorithm [15]. Especially, K. Zhang *et al.* [16] introduced the DnCNN architecture is well-known for effective noise reduction. Commonly, the oracle shrink method [17], visu shrink method [18], and bayes shrink method [19] are used to determine the thresholding value for noise reduction. However, these methods are suffered from the optimization to find the adaptive thresholding range. The DnCNN architecture can exquisitely separate the noise component by training the threshold value each of artificial neurons. Moreover, the convolution filters in each of perceptrons transfer to the variety sparsity domain, compared to the discrete cosine transform and wavelet transform and its process is helping to decide the accurate thresholding value.

The purpose of this study was to develop a Deep-CNN noise reduction algorithm and investigate its performances in DWI. For that purpose, we used a 1.5- and a 3.0-T MRI systems and imaged a chicken breast phantom. To evaluate the noise characteristics quantitatively, in this study, the root-mean-square error (RMSE), structural similarity (SSIM), contrast-to-noise ratio (CNR), and coefficient of variation (COV) were used.

2. Materials and Methods

2.1. Proposed framework for noise reduction in the DWI data

In MRI systems, image degradation occurs because of the inherent characteristics of the combination of the original signal and external signal (for example, noise). Image restoration is based on the deterioration characteristics of the imaging system, which can be simply modeled as follows:

$$I(m, n) = (f(m, n)\cos(\theta(m, n)) + n_{Re}(m, n)) + i(f(m, n)\sin(\theta(m, n)) + n_{Im}(m, n)), \quad (2)$$

where $I(m, n)$ is a degraded image signal, $f(m, n)$ is the signal from a region of interest (ROI), $\theta(m, n)$ denotes the phase difference of each pixel, and $n_{Re}(m, n)$ and $n_{Im}(m, n)$ represent the Gaussian white noise in the real and imaginary parts, respectively. Therefore, the value the will be visualized is the magnitude of $I(m, n)$, which can be rewritten as follows:

$$|I(m, n)| = \sqrt{\begin{matrix}(f(m, n)\cos(\theta(m, n)) + n_{Re}(m, n))^2 \\ + i(f(m, n)\sin(\theta(m, n)) + n_{Im}(m, n))^2\end{matrix}}. \quad (3)$$

Nonlocal self-similarity models are well-known noise reduction algorithms [20, 21]. Especially, the NLM algorithm is computed as in Eq. (4):

$$y(s) = \frac{1}{Z(s)}\Sigma_{t \in N(s)} w(s, t)[f(z)](t), \quad (4)$$

where $Z(s)$ is a normalized constant of $w(s, t)$, $N(s)$ is a large search window centered at pixel s, $w(s, t)$ indicates the similarity between two square patches δ_s and δ_t centered at s and t, respectively, and is defined as follows:

$$w(s, t) = \exp\left(-\frac{g(s, t)}{d^2}\right), \; g(s, t) = \frac{1}{\delta}\|y(\delta_s) - y(\delta_t)\|_2^2. \quad (5)$$

However, these techniques have high computation costs due to the calculation of the complex optimization and cannot prevent edge smoothing. In the last few years, outstanding results have been reported with the application of advanced neural network methods [22, 23]. Particularly, Deep-CNN is a machine-learning method that exploit multiple layers of non-linear information processing [24]. To successfully separate the noise component, we used the DnCNN architecture, which consists of convolution layers (in our case, 3 × 3 convolutional filters), batch normalization [25], and ReLU [26], acting as the activation function. The loss function is implemented by means of back-propagation with adaptive moment estimation (ADAM) [27]. For training, the model noisy images were designed using *imnoise*(·) functions (we used $\sigma = 1$ to 10, empirically) in the MATLAB toolbox (version 8.3, MathWorks, Natick, Massachusetts, USA). Here, the clean images were preparation for training sets those are composed of noise-free DWI data from 2,500 views. We generated the 30,420,000 image patches at the condition of 10 stride (*i.e.*, the image size is 448 × 448 pixels). And then we designed the training sets (*i.e.*,

Table 1. Training conditions of the Deep-CNN in simulations and experiments.

Environment	Specification
Training slices	2500 (5% used for validation, 2% used for test)
Image size	448 × 448
Patch size	64
Batch size	10
Epoch	150
Stride	2
Number of layers	15
Number of channels	64
Size of convolution filter	3 × 3
Learning rate	10^{-3}
Method for loss function	ADAM

simulated noise patches and their noisy patches) depending on the sigma values. Here, the 125 views among the 2500 views are used for the validation and 50 views among the total views are used for the test to calculate the accuracy. In this training, the root-mean square error between the label data and predicted data indicated about 2×10^{-3}. The training conditions are listed in Table 1.

The noise-free DWI data have a standard deviation of approximately 1.68 and we can assume that the noise component was in the range of approximately −5.04 to 5.04 because it follows a normal distribution (*e.g.*, 99.7 % of the noise component is within the range of $-3\eta(x)$ to $3\eta(x)$). The range of noise in the 12-bit pixel value ratio was approximately 0.1 %, is negligible.

Fig. 1 shows a simplified flowchart of the Deep-CNN-based noise reduction algorithm for DWI. In brief, in the training scheme, the clean images generated noisy images and then directly subtracted the clean images to obtain noise images. Then, the Deep-CNN architecture is applied and the parameters of the network architecture are estimated to extract the noise component. After the training, the noisy image is fed to the trained Deep-CNN architecture to obtain the residual image, which includes the noise component. Finally, the restored image is calculated and subtracted from the noisy image.

2.2. MRI devices and phantom

For acquiring diffusion-weighted images, we used a 1.5-T (Espree, Siemens, Germany) and a 3.0-T (Skyra, Siemens, Germany) MRI device. The 1.5- and 3.0-T MRI devices were used with 8 and 20 channel coils, respec-

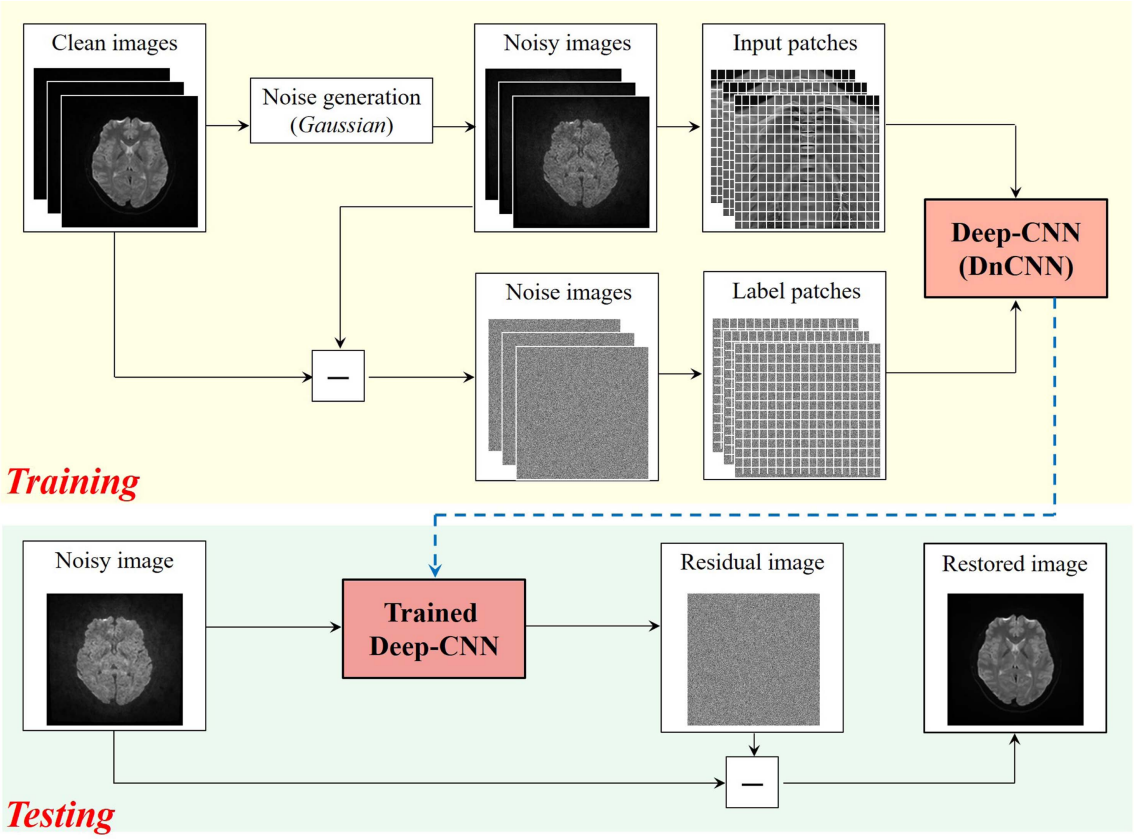

Fig. 1. (Color online) Simplified flowchart of the Deep-CNN-based noise-reduction algorithm for DWI.

Table 2. MRI data acquisition parameters.

Scan parameter	1.5 T	3.0 T
Coil channel	8	20
Repetition time (TR, msec)	4,000	5,500
Time to echo (TE, msec)	83	110
Field of view (FOV, mm^2)	240 × 240	
Number of excitation (NEX)	2	
Slice thickness (mm)	3	
Gap (mm)	0.6	
Phase encoding direction	Right to left	

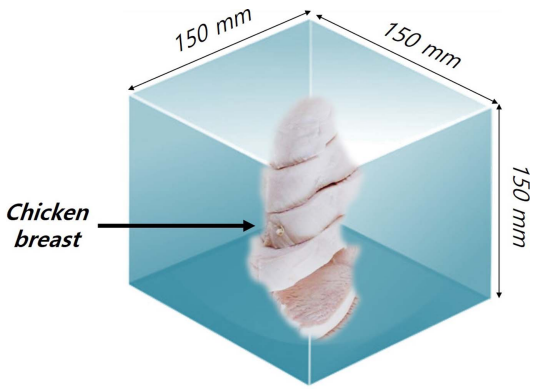

Fig. 2. (Color online) Photograph and dimensions of the chicken breast phantom.

tively. We used the echo planar imaging pulse sequence for DWI; Table 2 shows the MR acquisition parameters. In addition, we manufactured a chicken breast phantom using a cylindrical plate with a 100-mm height and 50-mm diameter in a 150 × 150 × 150 mm^3 acrylic plate. To minimize the interface between tissues and air, distilled water was poured into the cylindrical plate. Fig. 2 shows a photograph of the chicken breast phantom.

2.3. Image quality analysis

The image characteristics in terms of the profile, RMSE, SSIM, CNR, and COV were investigated quantitatively. The RMSE is defined as the difference between the data of the gold standard image ($\mu_{x,y}$) and the estimated image ($\hat{\mu}_{x,y}$):

$$RMSE(x, y) = \sqrt{\frac{\Sigma_{i=1}^{N}(\mu_{x,y} - \hat{\mu}_{x,y})^2}{\Sigma_{i=1}^{N}(\hat{\mu}_{x,y})^2}}, \quad (6)$$

where (x, y) are the indexes of the data in the image domain. Here, the smaller is the RMSE, the greater is the resemblance to the gold standard image. The SSIM factors can be expressed mathematically as follows:

$$SSIM(x, y) = l(x, y)c(x, y)s(x, y), \quad (7)$$

$$SSIM(x, y) = \frac{(2\mu_x\mu_y + C_1)(2\sigma_{xy} + C_2)}{(\mu_x^2 + \mu_y^2 + C_1)(\sigma_x^2 + \sigma_y^2 + C_2)}, \quad (8)$$

where the SSIM is based on three components: luminance (l), contrast (c), and structure (s). μ_x and μ_y are the local means in the x and y directions, respectively, σ_x and σ_y are the standard deviations in the x and y directions,

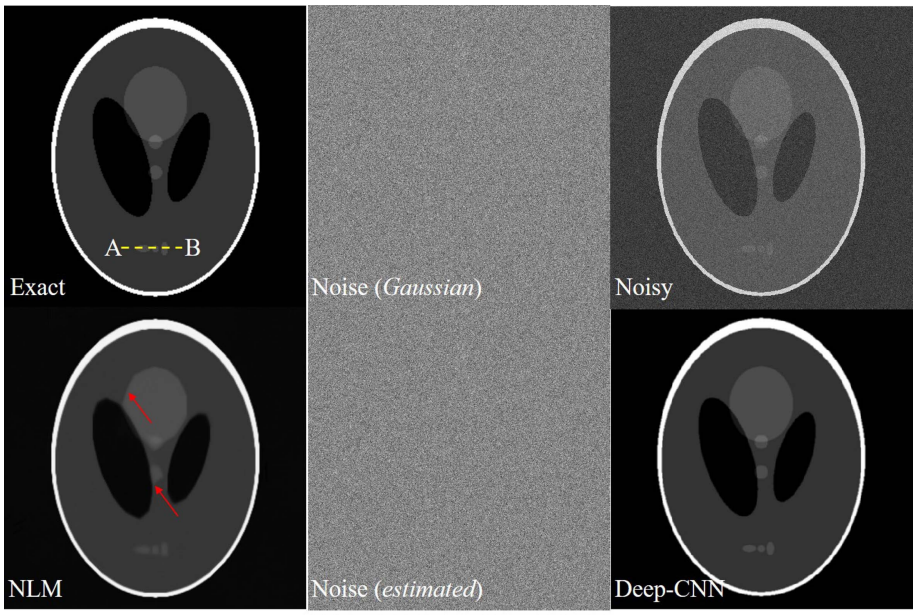

Fig. 3. (Color online) Simulation results of exact image (top left), generated Gaussian noise image (top middle), noisy image (top right), restored image using the non-local mean (NLM) algorithm (bottom left), estimated noise image using Deep-CNN (bottom middle), and restored image using Deep-CNN (bottom right).

respectively, and σ_{xy} is the cross-covariance in the image domain. C_1 and C_2 are constants between zero and one. The closer these constants are to 1, the closer the image is to the exact image. The details of the SSIM have been investigated extensively in the literature [28]. The CNR is defined as follows:

$$CNR = \frac{\bar{\mu}_{ROI_1} - \bar{\mu}_{ROI_2}}{\bar{\sigma}^2_{ROI_1} - \bar{\sigma}^2_{ROI_2}}, \quad (9)$$

where $\bar{\mu}$ and $\bar{\sigma}$ are the mean and standard deviation in the ROI (a rectangular ROI in our case; for example, ROI_1 and ROI_2 in Fig. 5), respectively. Here, the CNR value shows the characteristic of the contrast considering noise fluctuations in the ROI. The COV can be expressed as follows:

$$COV = \frac{\sigma}{\mu}. \quad (10)$$

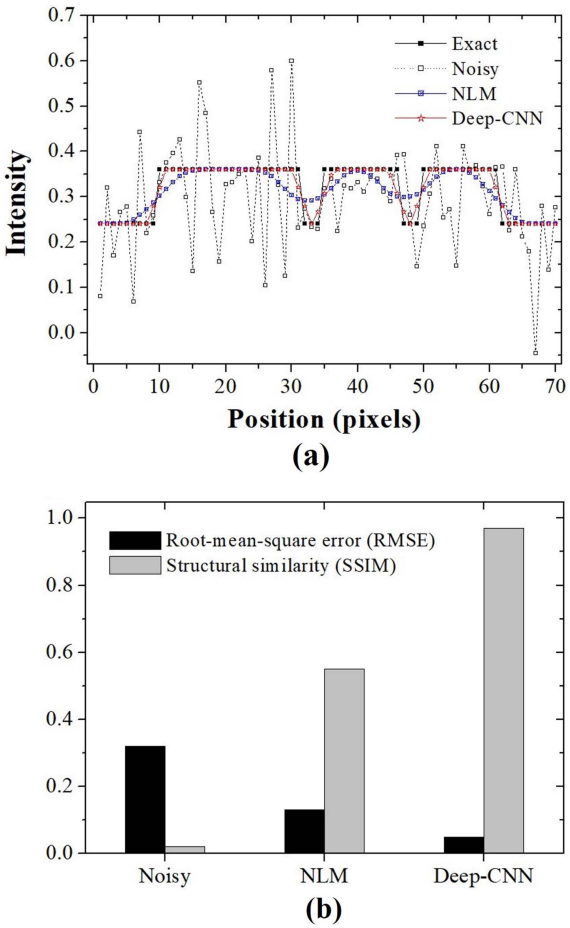

Fig. 4. (Color online) (a) 1D intensity profiles measured along the $\overline{AB}$ line segments indicated in Fig. 3 and (b) the measured RMSE and SSIM values from the simulation images in Fig. 4 for the noisy, restored with NLM, and restored with Deep-CNN cases.

The COV is also called the "*coefficient of dispersion*" [29] and a small COV value indicates a higher image quality because this factor reflects the noise fluctuations in the image domain.

3. Results and Discussion

Fig. 3 shows the simulation results of the exact image (top left), the generated Gaussian noise image (top middle), the noisy image (top right), the image restored using the NLM (bottom left), the noise image estimated using the Deep-CNN (bottom middle), and the image restored using Deep-CNN (bottom right). Note that the image restored using Deep-CNN presents higher quality than the noisy and restored images using the NLM algorithm. Fig. 4(a)

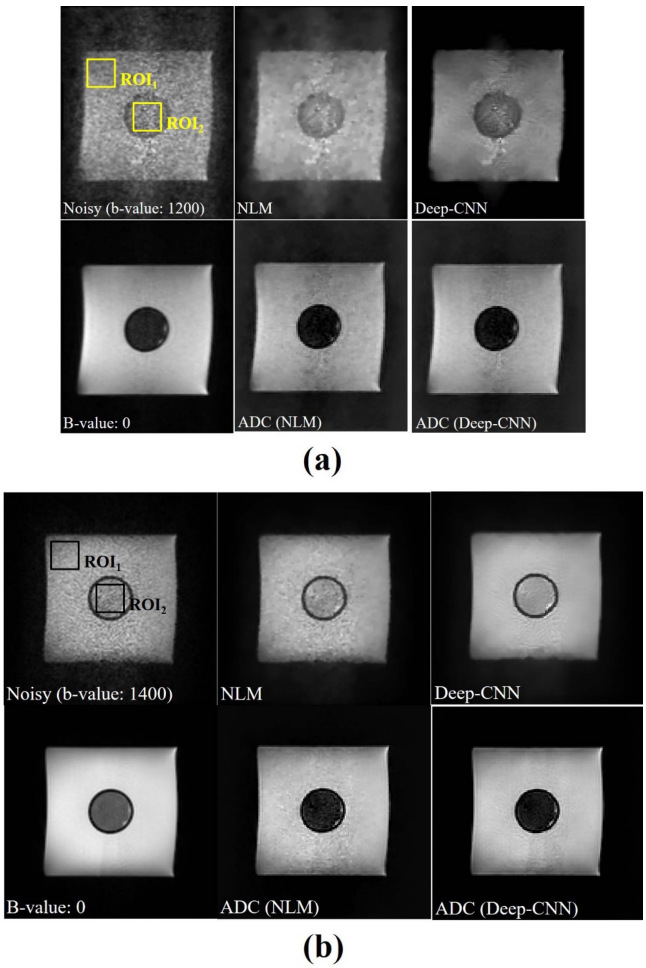

Fig. 5. (Color online) Experiment results of noisy image (top left), image restored using NLM (top middle), image restored using Deep-CNN (top right), clean image with b-value of zero (bottom left), ADC map from the clean image and restored image using NLM (bottom middle), and ADC map from the clean image and restored image using Deep-CNN (bottom right); (a) 1.5 T and (b) 3.0 T.

shows the intensity profiles measured along the $\overline{AB}$ line segments indicated in Fig. 3. Note that, compared to the image restored using the NLM algorithm, the profile of the image restored using the Deep-CNN is much closer to that of the exact image. For the quantitative evaluation, we measured the RMSE and SSIM characteristics and the results are reported in in Fig. 3(b). The RMSE values are approximately 0.32 (noisy image), 0.13 (restored image using NLM), and 0.05 (restored image using Deep-CNN. The SSIM values were approximately 0.02 (noisy image), 0.55 (restored image using NLM), and 0.97 (restored image using Deep-CNN). These results indicate that the proposed framework was very effective in reducing the noise component of the magnetic resonance images.

Fig. 5 shows the experiment results of the noisy image (top left), the image restored using the NLM (top middle), the image restored using Deep-CNN (top right), the clean image with a b-value of zero (bottom left), the ADC map from the clean image and the image restored using NLM (bottom middle), and the ADC map from clean image and the image restored using Deep-CNN (bottom right). Here, (a) and (b) are obtained in the 1.5 and 3.0 T condition. Note that the restored and ADC images using the Deep-CNN are much more clearly visible then the restored and ADC images using the NLM algorithm. Fig. 6 shows the CNR and COV values in the (a) 1.5 T and (b) 3.0 T conditions. Here, we predefined the ROI_1 and ROI_2 in Fig. 5. The CNR values in the 1.5 T images were approximately 1.75 (noisy image), 5.78 (image restored using NLM), and 7.15 (image restored using Deep-CNN), while in the 3.0 T images they were 3.72 (noisy image), 6.63 (image restored using NLM), and 9.11 (image restored using Deep-CNN). Furthermore, the COV values of the 1.5 T images were approximately 0.98 (noisy image), 0.52 (restored image using NLM), and 0.31 (restored image using Deep-CNN) and those of the 3.0 T images were 0.57 (noisy image), 0.26 (restored image using NLM), and 0.14 (restored image using Deep-CNN). Note that, compared to all other images, the image restored using the proposed framework exhibits a superior noise-suppression performance, while preserving the edge structure in the MRI.

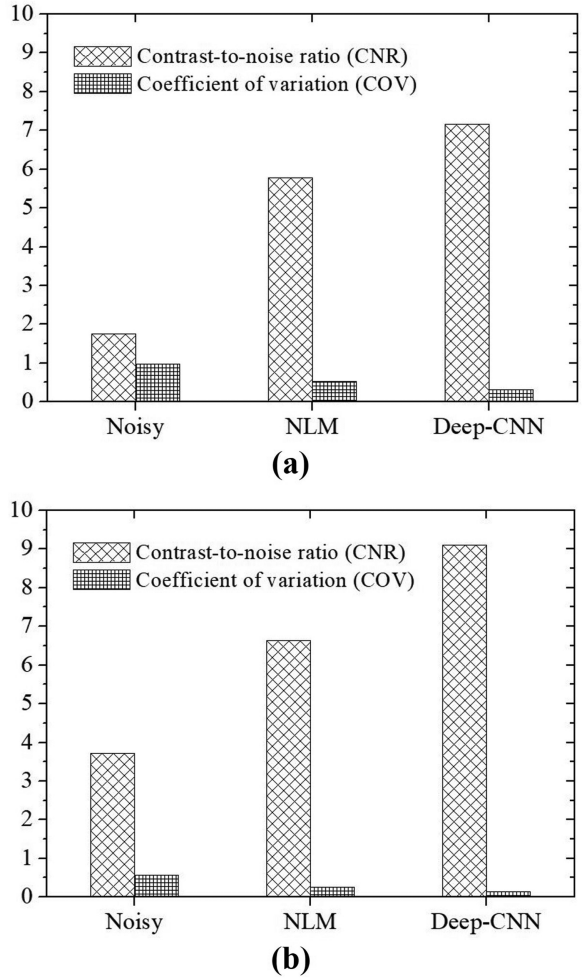

Fig. 6. Measured CNR and COV indicated by predefining region-of-interests (ROIs) (*i.e.*, ROI_1 and ROI_2 in Fig. 5); (a) 1.5 T and (b) 3.0 T.

4. Conclusion

In this study, we investigated and analyzed the proposed Deep-CNN-based noise-suppression framework in DWI. We validated the proposed scheme by performing simulations and experiments. According to our results, the RMSE values of the images restored using Deep-CNN was approximately 6 and 2 times smaller than those of other images and the SSIM value of the image restored using the proposed scheme was approximately 50 and 2 times higher than those of images in the simulation. Especially, the inner structures of the numerical phantom were sharper in the image restored using Deep-CNN than in all other images. Moreover, the CNR values of images processed with the proposed algorithm were approximately 1.3 times higher than those of the images restored using the NLM algorithm. The COV values also improved by factors of approximately 2, compared to those of the images restored using the NLM algorithm. In conclusion, our results indicated that the proposed scheme is effective in DWI noise reduction.

Acknowledgment

The research was supported by the National Research Foundation of Korea (NRF-2016R1D1A1B03930357)

and the Gachon University research fund of 2018 (GCU-2018-0289). Dong-Kyoon Han and Kyuseok Kim contributed equally to the writing of this paper.

References

[1] European Society of Radiology, Insights Imaging **6**, 141 (2015).
[2] J. H. Thrall, Radiology **279**, 660 (2016).
[3] M. Mascalchi, G. Belli, M. Zappa, G. Picozzi, M. Falchini, R. D. Nave, G. Allescia, A. Masi, A. L. Pegna, N. Villari, and E. Paci, AJR **187**, 421 (2006).
[4] M. S. Cho, J. H. Cho, Y. M. Chang, Y. H. Cho, S. K. Zeon, K. R. Dong, W. K. Chung, H. K. Lee, H. J. Kim, J. Y. Bae, J. O. Ahn, and S. J. Lee, J. Magn. **16**, 350 (2011).
[5] Y. Lee, M. H. Choi, H. J. Goh, and D. K. Han, J. Magn. **21**, 281 (2016).
[6] R. J. Russo, H. S. Costa, P. D. Silva, J. L. Anderson, A. Archad, R. W. W. Biederman, N. G. Boyle, J. V. Frabizzio, U. B. Green, S. L. Higgins, R. Lampert, C. E. Machado, E. T. Martin, A. L. Rivard, J. C. Rubenstein, R. H. M. Schaerf, J. D. Schwartz, D. J. Shah, G. F. Tomassoni, G. T. Tominaga, A. E. Tonkin, S. Uretsky, and S. D. Wolff, N. Engl. Med. **376**, 755 (2017).
[7] M. A. Schmidt and G. S. Payne, Phys. Med. Biol. **60**, R323 (2015).
[8] D. M. Koh, D. J. Collins, and M. R. Orton, AJR **196**, 1351 (2011).
[9] D. M. Koh and D. J. Collins, AJR **188**, 1622 (2007).
[10] A. R. Padhani, G. Liu, D. M. Koh, T. L. Chenevert, H. C. Thoeny, T. Takahara, A. D. Jurasz, B. D. Ross, M. V. cauteren, D. Collins, D. A. Hammoud, G. J. S. Rustin, B. Taouli, and P. L. Choyke, Neoplasia **11**, 102 (2009).
[11] M. C. Maas, J. J. Futterer, and T. W. J. Scheenen, Invest. Radiol. **48**, 779 (2013).
[12] M. Kazubek, IEEE Signal Proc. Let. **10**, 324 (2003).
[13] L. Rudin, S. Osher, and E. Fatemi, Physica D **60**, 259 (1992).
[14] A. Buades, B. Coll, and J. Morel, Multiscale Model. Simul. **4**, 490 (2006).
[15] H. Chen, Y. Zhang, W. Zhang, P. Liao, K. Li, J. Zhou, and G. Wang, 2017 IEEE 14th International Symposium on Biomedical Imaging, 143 (2017).
[16] K. Zhang, W. Zho, Y. Chen, D. Meng, and L. Zhang, IEEE Trans. Image Process **26**, 3142 (2017).
[17] S. G. Chang, B. Yu, and M. Vetterli, IEEE Trans. Image Process **9**, 1522 (2000).
[18] D. L. Dononho and I. M. Johnstone, Biometrika. **81**, 425 (1994).
[19] F. Ruggeri and B. Vidakovic, Statist. Sinica. **9**, 183 (1999).
[20] K. Dabov, A. Foi, V. Katkovnik, and K. Egiazarian, IEEE T. Image Process **16**, 2080 (2007).
[21] Y. Liu, J. Wang, C. Xi, Y. Guo, and Q. Peng, The proceedings of 10th IEEE International Conference on Computer-Aided Design and Computer Graphics (2007).
[22] C. Szegedy, W. Liu, Y. Jia, P. Sermanet, S. Reed, D. Anguelov, D. Erhan, V. Vanhoucke, and A. Rabinovich, In Proceedings of IEEE International Conference on Computer Vision and Pattern Recognition, 1 (2015).
[23] K. He, X. Zhang, S. Ren, and J. Sun, In Proceedings of IEEE International Conference on Computer Vision and Pattern Recognition, 770 (2016).
[24] W. Rawat and Z. Wang, Neural Comput. **29**, 2352 (2017).
[25] S. Ioffe and C. Szegedy, In Proc. International Conference on Machine Learning (ICML 2015), 448 (2015).
[26] A. Krizhevshy, I. Sutskever, and G. Hinton, In Advances in Neural Information Processing Systems 25 (NIPS 2012), 1097 (2012).
[27] D. P. Kingma and J. Ba, 3rd International Conference for Learning Representations, San Diego (2015), arXiv: 1412.6980v9.
[28] Z. Wang, A. C. Bovik, H. R. Sheikh, and E. P. Simoncelli, IEEE T. Image Process. **13**, 600 (2004).
[29] C. E. Brown, Coefficient of Variation (Chapter 13). in applied multivariate statistics in geohydrology and related sciences, Springer, Berlin, Heidelberg (1998).